Measurements of Pulmonary Vascular Permeability with PET and Gallium-68 Transferrin

Mark A. Mintun, Darrell R. Dennis, Michael J. Welch, Carla J. Mathias, and Daniel P. Schuster

Mallinckrodt Institute of Radiology and the Department of Internal Medicine, Washington University School of Medicine, St. Louis, Missouri

We quantified pulmonary vascular permeability with positron emission tomography (PET) and gallium-68- (^{68}Ga) labeled transferrin. Six dogs with oleic acid-induced lung injury confined to the left lower lobe, two normal human volunteers, and two patients with the adult respiratory distress syndrome (ARDS) were evaluated. Lung tissue-activity measurements were obtained from sequential 1–5 min PET scans collected over 60 min, after in vivo labeling of transferrin through intravenous administration of [^{68}Ga]citrate. Blood-activity measurements were measured from simultaneously obtained peripheral blood samples. A forward rate constant describing the movement of transferrin from pulmonary vascular to extravascular compartments, the pulmonary transcapillary escape rate (PTCER), was then calculated from these data using a two-compartment model. In dogs, PTCER was 49 ± 18 in normal lung tissue and 485 ± 114 10^{-4} min^{-1} in injured lung. A repeat study in these dogs 4 hr later showed no significant change. Values in the human subjects showed similarly marked differences between normal and abnormal lung tissue. We conclude that PET will be a useful method of evaluating vascular permeability changes after acute lung injury.

J Nucl Med 28:1704–1716, 1987

The pathogenesis of pulmonary edema is commonly attributed to either cardiogenic or noncardiogenic causes. During heart failure, the pulmonary capillary hydrostatic pressure is elevated, and the convective flow of relatively protein-poor fluid across the alveolo-capillary membrane is increased. When the etiology of pulmonary edema is noncardiogenic, the sieving property of the pulmonary capillary endothelium is altered, and both the flux of protein and water into the extravascular space is increased. Under these circumstances, the capillary hydrostatic pressure is usually normal. Clinically, therefore, the diagnosis of "increased permeability" pulmonary edema is generally made by inference; when pulmonary edema occurs in the setting of normal hydrostatic pressures (estimated from pulmonary artery wedge pressures), the pathogenesis is generally assumed to be noncardiogenic in origin.

This approach to diagnosis is unsatisfactory for several reasons. First, both the permeability to protein macromolecules and the pulmonary wedge pressure can be elevated at the same time. Second, therapy initiated prior to pulmonary artery catheterization can have a profound effect on the wedge pressure measurement, leading to potentially spurious deductions about pathogenesis. Third, increases in permeability may cover a broad spectrum of values which cannot be evaluated by simple inferences from wedge pressure measurements. Finally, changes in permeability prior to the onset of clinically obvious pulmonary edema, or during the course of its resolution, cannot be made without a direct measurement of permeability itself. For all these reasons, a quantitative measure of pulmonary vascular permeability (PVP) would be desirable.

In 1978, Gorin et al. (*1*) reported a means for measuring the flux of a radiolabeled protein across the pulmonary endothelium by external radiation detection. The technique was validated by comparing the calculated index of vascular permeability with direct measurements of protein flux into lung lymph in sheep, and later on, the method was adapted for use in humans (*2*). Gorin et al. used two tracers (of different photon

Received Oct. 8, 1986; revision accepted May 11, 1987.

For reprints contact: Daniel Schuster, MD, Respiratory and Critical Care Division, Box 8052, Washington University School of Medicine, 660 S. Euclid, St. Louis, MO 63110.

energy) injected intravenously, and a NaI scintillation detector to measure radioactivity over a region of lung. One tracer (^{99m}Tc-labeled autologous red blood cells) was used as a blood-pool reference, while the other (indium-113m transferrin) was used to follow the flux of protein from the vascular to extravascular space. Tissue-activity measurements were then obtained during a 1–2 hr period, and a rate constant (referred to as the pulmonary transcapillary escape rate for transferrin, or PTCER) was calculated. Thus, this approach allowed a direct, quantitative measure of PVP.

External radiation measurements can also be made with positron emission tomography (PET). Besides the quantitative power of PET, tomography also allows the PTCER measurement to be displayed regionally, and to be correlated with other PET-derived measurements relevant to lung injury (e.g., extravascular lung water or regional pulmonary blood flow). Therefore, in this report, we demonstrate that Gorin's method for measuring PTCER can be successfully adapted for use with PET. In dogs, we show that the measurement is reproducible, and will distinguish normal from abnormal areas of lung when injury is nonhomogeneous. In four human subjects, we show that the same technique can readily distinguish lung injured by the adult respiratory distress syndrome (ARDS) from normal lung.

METHODS

Theory

After the i.v. injection of a radiolabeled protein such as transferrin, rapid equilibration within the intravascular blood pool is followed by a slow egress of the protein macromolecule from blood into the extravascular space. The time required for eventual equilibration between intra- and extravascular spaces is dependent on both the local capillary endothelial permeability to that protein, and on the surface area available for efflux. If both the plasma time-activity and the local extravascular time-activity curve is known, a protein permeability-surface area product for a given tissue can be calculated (see Appendix). The major assumption involved in such a calculation is that the movement of protein across the endothelium results solely from passive, not active, forces.

Since external detection cannot distinguish whether the activity from the radiolabeled protein is localized to either intravascular or extravascular compartments, the accumulation of activity in the extravascular space can only be determined by estimating the intravascular activity separately and subtracting it from the total measured value. As previously noted, Gorin et al. (*1–2*) used a second, simultaneously administered vascular tracer in addition to the radiolabeled protein to provide such information. This strategy is not possible with PET since the photons detected as a result of any positron emission are mono-energic (511 keV). Instead, assuming that all activity is confined to the vascular pool at time zero (the time of intravenous administration), vascular volume, and rate constants between vascular and extravascular compartments can be calculated simultaneously by parameter estimation techniques (see Appendix). Obviously, this approach also assumes that blood volume does not change during the scan period, since the local tissue intravascular activity at any given time during the scan is assumed to equal the estimated local tissue blood volume multiplied by the blood activity obtained from peripheral blood sampling.

The model originally proposed by Gorin allowed calculation of both forward (k_1) (vascular to extravascular) and reverse (k_2) transport rate constants (Fig. 1). Both constants are directly influenced by the surface area available for protein transport. In the lung, with varying amounts of lung tissue per unit volume, measured k_1 and k_2 would vary accordingly. However, assuming that regional blood or plasma volume will vary linearly with surface area, the rate constants can be normalized to changes in surface area by dividing each by the regionally specific blood or plasma volume. Gorin et al. termed this normalized value for the forward constant, the pulmonary transcapillary escape rate, or PTCER (i.e., PTCER = k_1/Vpl, where Vpl is regional plasma volume). Units are typically expressed as fractional change over time for PTCER (min^{-1}), or volume of tracer "cleared" over time for k_1 ($ml \cdot min^{-1}$). The reverse rate constant represents return of activity into the intravascular pool through either backdiffusion or lymphatic drainage. To calculate both forward and reverse rate constants, data must be collected over an extended period of time, and an iterative parameter estimation procedure must be used (see Appendix).

Alternatively, back-flux of the radiolabeled protein can be assumed to be negligible during the scan. With this simplification, linear regression techniques may be used to calculate PTCER (see Appendix), which considerably shortens the computational time required for the calculation, and makes it possible to create tomographic images of PTCER. Even if back-flux of the tracer protein is significant, PTCER can still be accurately calculated with linear regression models if data collection is kept appropriately short, i.e., is stopped before backdiffusion of the labeled protein significantly affects the time-activity curve (Fig. 2). If this approach is taken, however, k_2 cannot be calculated, and therefore its influence or importance cannot be evaluated.

PET Techniques

All animal studies were performed on PETT-VI. Specifications of this device have been reported elsewhere (*3–4*). Briefly, seven slices of data are collected simultaneously by multiple rings of cesium fluoride detectors with an intrinsic

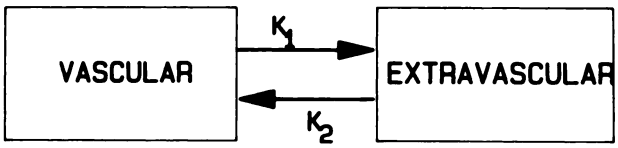

FIGURE 1
Schematic diagram of the two-compartment model used to evaluate tissue activity measurements obtained with PET after i.v. injection of ^{68}Ga-labeled transferrin. k_1 and k_2 are forward and reverse rate constants, respectively. If the volume of the vascular compartment and the hematocrit is known, then the pulmonary transcapillary escape rate (PTCER) can be calculated as k_1/Vpl, where Vpl is plasma volume in the ROI.

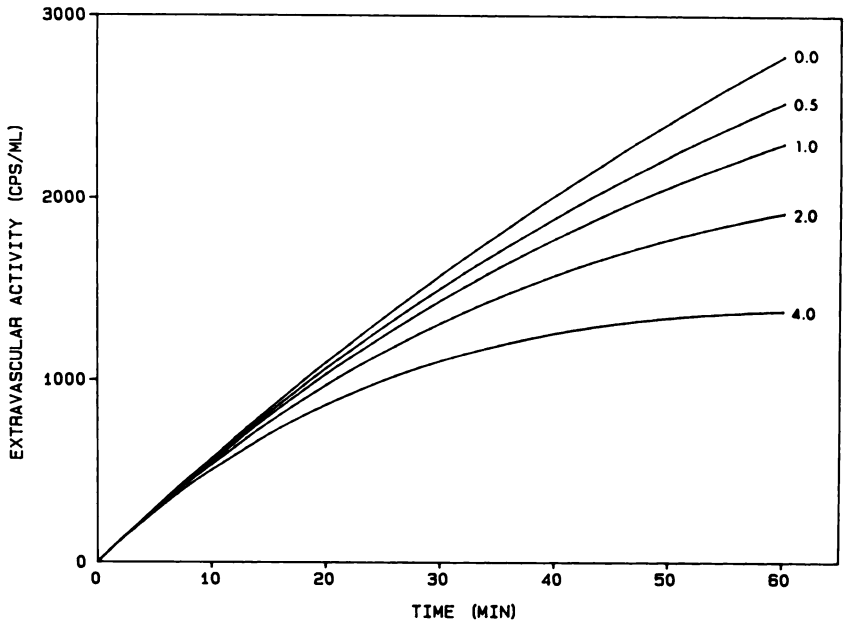

FIGURE 2
Computer simulation of the effects of k_2 on the time-extravascular tissue activity relationship, using the model in Figure 1 and Eq. (14) of the Appendix. For this simulation, k_1 was arbitrarily given a value of 1.0 10^{-4} sec^{-1} and k_2 was given values varying from 0.5 to 4.0 10^{-4} sec^{-1} (similar to actual values measured in injured lung, Table 1). Note that the curves begin to diverge significantly from one another ~20 min after entry of the tracer into the intravascular compartment. Thus, as k_2 becomes larger, fitting such data with models that assume k_2 to be zero, will clearly lead to a poor estimation of the initial behavior of the time-activity relationship. This, in turn, should lead to an inaccurate estimation of k_1 (and PTCER).

in-plane resolution of 11.7 mm full width at half maximum (FWHM). After image reconstruction by filtered backprojection, images with an 18-mm resolution (FWHM) are obtained. Slice thickness is ~14 mm (FWHM).

Human studies were performed on a SUPER-PETT I tomograph (*5*). This device collects seven simultaneous slices using multiple rings of cesium and barium fluoride detectors with an intrinsic in-plane resolution of 11.4 mm. Image reconstruction, in this case, yields an in-plane resolution of 15 mm FWHM.

In using both types of scanners, blank and transmission scans were obtained before collecting subsequent emission scans. The transmission scan was obtained with a ring of $^{68}Ge/^{68}Ga$ activity encircling the subject. This scan was then used to correct the later PET data collection for the effects of attenuation. Furthermore, since attenuation of the positron annihilation photons is proportional to tissue density, appropriately scaled transverse tomographic images of lung density can be created (*17*). These images can then be used to accurately place regions of interest (ROIs) within normal or abnormal lung tissue in other PET scans.

All reconstructed images were corrected for decay back to the time of isotope injection and calibrated against images of a phantom containing various concentrations of carbon-11 bicarbonate.

During all emission scans, blood samples were obtained and the radioactivity in these samples was immediately determined in a NaI(Tl) well-counter. These samples were obtained through a femoral arterial catheter in dogs, and through an antecubital or femoral vein catheter in human subjects. Blood activity was decay corrected to the time of injection and expressed as cts/sec/ml blood, assuming a blood density of 1.05 g/ml blood. After discarding the first 2 min of data, a curve-stripping technique was used to find the best fit for the measured blood time-activity points. Initial attempts to describe the blood curve data with a mono-exponential curve did not reliably fit the actual blood-activity data for the first 10 min after isotope administration. Therefore, this approach was abandoned in favor of using a bi-exponential fit.

Isotope Preparation

Gallium-68 citrate was produced by mixing 0.5 ml of [^{68}Ga] chloride from a $^{68}Ge/^{68}Ga$ generator (*6–7*) and 4.0 ml of normal saline in a citrated Vacutainer (R) tube. After intravenous injection, the ^{68}Ga rapidly exchanges and binds to native transferrin with a very high stability constant (*8*).

General Animal Preparation

Six mongrel dogs weighing 20 to 28 kg were anesthetized with 25–30 mg/kg of intravenously administered pentobarbital and paralyzed with 4 mg pancuronium given intravenously. The dogs were ventilated through an endotracheal tube with a Harvard pump respirator at 15 ml/kg tidal volume and a rate adjusted to bring the arterial PCO_2 and pH within the normal range. A balloon-tipped flotation catheter was placed into the pulmonary artery under fluoroscopic guidance; in addition, an arterial catheter was placed into the femoral artery.

Study Protocols

Dogs were placed supine into the PET device, with the most caudad slice located at the level of the diaphragm. A direct injection of oleic acid into the pulmonary circulation of the left lobe was used to create a localized area of pulmonary edema due to increased permeability. The oleic acid (0.01–0.02 ml/kg) was drawn up in 3 ml of 70% ethanol and injected through the distal lumen of the pulmonary artery catheter after balloon inflation and "wedging" of the catheter tip. In this way, injury was confined to approximately one-half of the left lower lobe. Ninety minutes later, 8 mCi of [^{68}Ga] citrate was injected intravenously and PET scans were obtained over the next 60 min. The scans were obtained as sequential 1-min collections during the first 20 min after injection, followed by ten 4-min collections. Blood samples, weighing ~0.5 g, were obtained from the femoral artery catheter throughout the scan period in 3-ml pre-weighed syringes. The hematocrit was determined by routine capillary tube centrifugation at the beginning of the scan. Approximately 4 hr after this first scan was completed, the procedure was repeated after injecting 10–15 mCi of [^{68}Ga]citrate.

Human studies were conducted in a similar fashion. These studies were approved by the institution's Human Studies Committee and the Radioactive Drug Research Committee. The subject was placed into the scanner supine with the most inferior slice at the level of the diaphragm. Separate intravenous catheters were placed for isotope administration and peripheral blood-activity measurements. The [^{68}Ga]citrate (8 mCi) was injected, and after 2 min 12 sequential 5-min PET scans were obtained. This protocol typically resulted in ~1.4 million and 0.6 million events per slice for scans at the beginning and end of the 60-min period, respectively. Peripheral blood samples were obtained during the scan as in the animal studies.

Image Analysis

Calculation of PTCER was carried out in three ways. In two of the methods (Methods A and B), ROIs (~1.3 cm on a side) were defined in a normal and in an injured portion of lung (dog experiments) as indicated by density measurements on the transmission scan. In the human subjects, two regions were chosen from typical dependent and nondependent regions of the lung. In these regions, tissue-activity curves were obtained from the sequential PET images and then analyzed with the bidirectional flux equation (Method B, Eqs. (14), (21), and (22), Appendix) to yield estimates of plasma volume (Vpl), k_1 and k_2, and the unidirectional flux equation (where $k_2 = 0$, Method A, Eqs. (17), (21), and (22), Appendix) to yield estimates of Vpl and k_1 only. Since when k_2 is assumed to be zero, errors in estimating k_1 increase as data from progressively longer periods of time are analyzed, (see Fig. 2), analysis by method A was limited to the first 20 min of data. For the third method, (Method C) which again assumes k_2 to be zero, linear regression equations, assuming uni-directional protein flux (Eqs. (19–22), Appendix), were used to calculate PTCER and Vpl for each pixel of the PET image, yielding a whole image map of PTCER and Vpl. Regional values of PTCER and Vpl were then recorded directly from the tomographic image, in the same ROIs used in Methods A and B. For all these calculations, the first 2 min of data after injection of the radiotracer was excluded from the analysis.

Statistical Analysis

Data are presented as the mean ± 1 s.d. Analysis-of-variance techniques were used to test for statistically significant differences ($p < 0.05$) between mean values. The GLM procedure of the Statistical Analysis System for the IBM-PC (SAS Institute, Cary, NC) was used for these calculations.

RESULTS

Figure 3 demonstrates typical regional tissue-time activity from a dog analyzed with method A (Figs. 3A and 3B) and method B (Fig. 3C). Only the extravascular tissue activity is plotted. For this illustration only, the curve fits applied to the data in Figure 3A were extended to include the full 60 min of data. While the quality of the computer generated fits for Methods A and B are indistinguishable for data taken from the *normal* lung region (solid circles), this is clearly not the case for the fits to the data from the abnormal lung (open circles). Method B, which estimates a plasma volume and both forward and reverse rate constants (k_1 and k_2) succeeds in fitting the tissue data well throughout the entire 60-min data collection. However, Method A, which assumes k_2 to be zero, visually fails to fit both the early steep initial rise in extravascular activity and the later slower rise in activity when all 60 min of data are used in calculating the curve fit. The actual fit obtained is some average of these and results in a lower k_1 estimation. Incidently, Method A, when used this way, also resulted in an overestimation of the plasma volume for this dog leading to the early negative values for extravascular activity. However, when Method A is used and the analysis is confined to the first 20 min of data, the curve fit is again excellent (Fig. 3B). Thus, these results reinforce the concerns previously discussed (see Theory section, see Fig. 2) and demonstrate the need to limit analysis of data through Method A (when k_2 is assumed to be zero) to only the first 20 min after tracer administration.

A single slice from the transmission scan of one animal is shown in Figure 4 to demonstrate the relevant anatomy. Images of single slices obtained at the same level as the transmission scan, 3 min and 60 min after injection of the [^{68}Ga]citrate, are also shown in Figure 4. The increase in tissue activity that occurs in the left lower lobe (LLL) after oleic acid-induced injury, compared with the rest of the lung, is evident.

Tissue-activity measurements, obtained from all 30 sequential PET scans in regions of interest placed over the injured area of lung in the LLL, from the same animal as in Figure 4, are plotted in Figure 5. Total, blood, and extravascular tissue-activity measurements are shown. Method B was used to fit the tissue curves shown. Using method C (similar to method A), PTCER was calculated on a pixel-by-pixel basis, and an image of the PTCER distribution for the same slice was created, also shown in Figure 4.

Mean data, comparing methods A and B, of calculating Vpl and PTCER are shown in Figures 6 and 7. No significant difference was found for the Vpl calculation by either method. However, in injured lung, Vpl decreased significantly from the first to the second measurement. No significant difference was found for PTCER values calculated by either method. Method C yielded identical results to Method A, as would be expected since the equations used to calculate PTCER and Vpl are mathematically similar. Mean values for the forward (k_1) and reverse (k_2) transport rate constants are given in Table 1; k_1 was significantly higher in injured lung compared with normal lung. However, values for k_2 were not statistically different.

Data from the human studies are given in Table 2. Values obtained in two normal human volunteers are

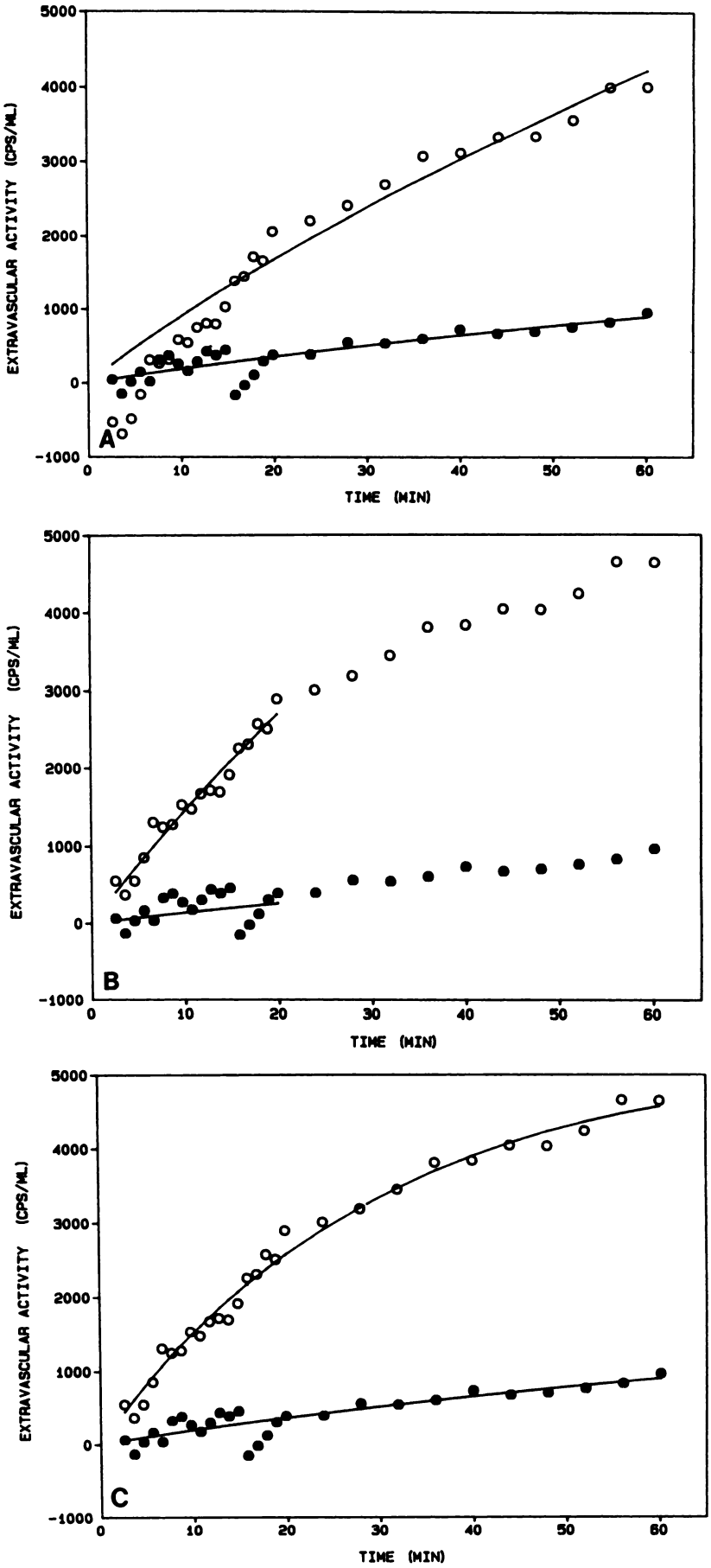

FIGURE 3
Time-extravascular tissue-activity data obtained from one representative animal. Data were obtained from one normal region (filled circles) and one region in injured lung (open circles). The solid line in each case represents the computer generated fit to the data. A: Method A (where k_2 is assumed to be zero, see methods) was used to fit curves to the data. All 60 min of data were used in these calculations. B: Method A again was used for the curve fit, but only the first 20 min of data were used for calculations. C: Method B (where both k_1 and k_2 are estimated) was used to fit the data. Clearly, Method A does not accurately describe the data if all 60 min of data are used. However, when either the analysis by Method A is confined to the first 20 min, or Method B is used, in which the influence of k_2 is taken into account, the curve fit is much improved.

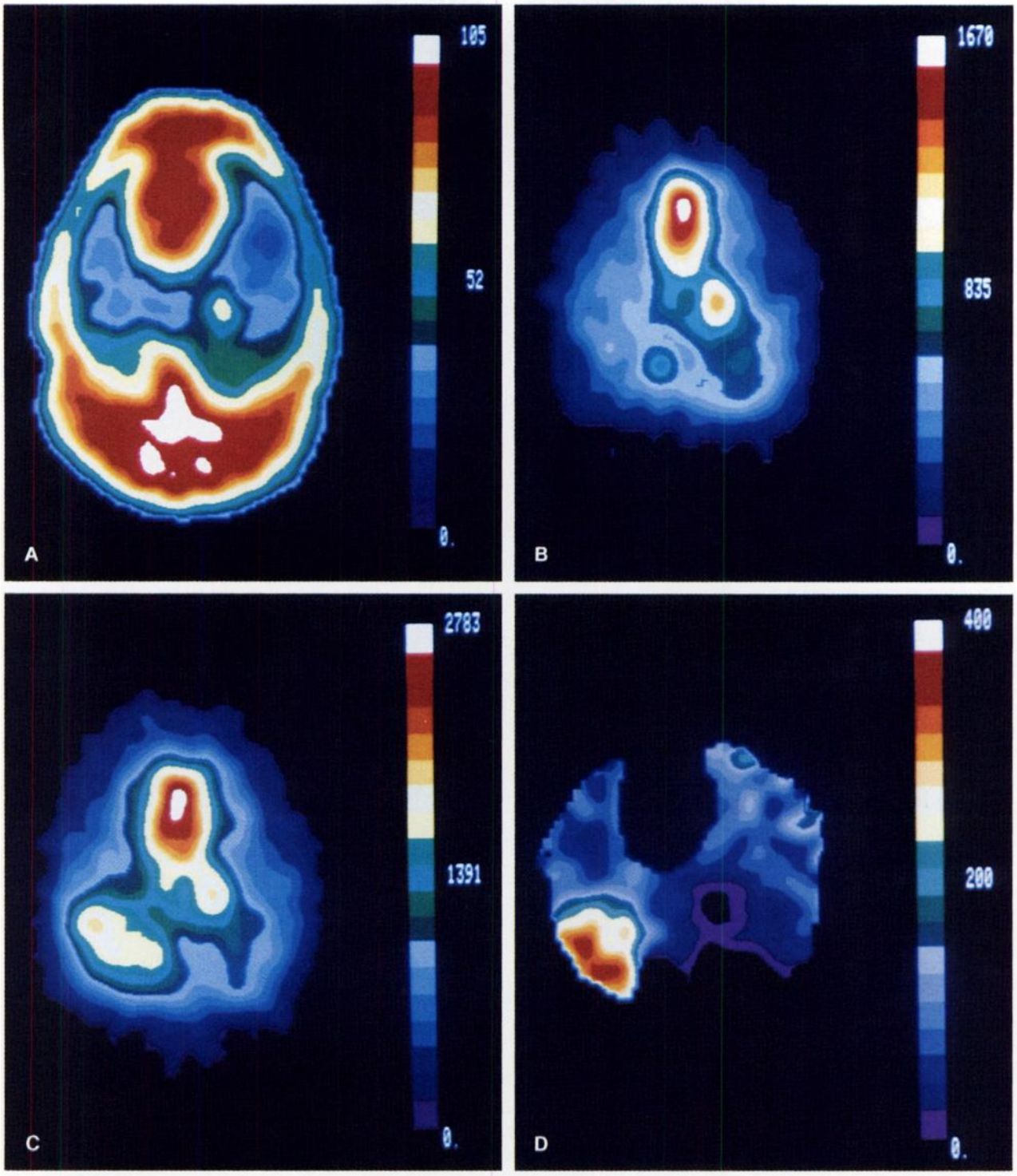

FIGURE 4

A: Single tomographic slice from a transmission scan from one dog, shown to depict the relevant anatomy. The color scale at the right has been scaled to units of tissue density (*17*,*18*) (g/100 ml lung). Note that the lung density varies between approximately 30 and 50 g/100 ml. For this and other PET images of dogs, the animal was supine, and the right side of the image is the right side of the dog. B: Tomographic image obtained from the same dog as in "A," at the same level, 3 min after i.v. injection of ^{68}Ga-labeled transferrin, and 90 min after oleic acid induced injury to the left lower lobe. Color scale at the right is in arbitrary PETT units. Note that at this early time, most of the activity is in vascular structures (heart, vena cava, and aorta). C: Image similar to "B," except obtained 60 min after injection of the labeled transferrin. Now note the marked increase in activity in the injured left lower lobe. D: PTCER image, obtained by analyzing all scans (as in "B" and "C") in a pixel-by-pixel basis, using Eq. (19) and (20) of the Appendix. Color scale at right is in units of 10^{-4} min^{-1}. Note the ~tenfold increase in PTCER in areas of injured lung compared with normal lung.

FIGURE 5
Time-tissue-activity plots of data obtained from the same animal shown in Figure 4. For this plot, only data from a region within injured lung were used. Circles: total tissue-activity obtained with PET. Each point represents data from one of 30 sequential PET scans. Method B (see text) was used to generate a fit to this data. Triangles: blood-activity measurements obtained from femoral artery blood samples. Each point represents one blood sample. Also shown is the bi-exponential curve fit to this data. After estimating the blood volume (Method B) in the lung ROI, blood activity during each of the 30 sequential PET scans was estimated from the blood volume estimate and the femoral artery blood-activity curve. Subtracting this data from the total tissue-activity measurements, yielded the extravascular tissue activity estimate (squares).

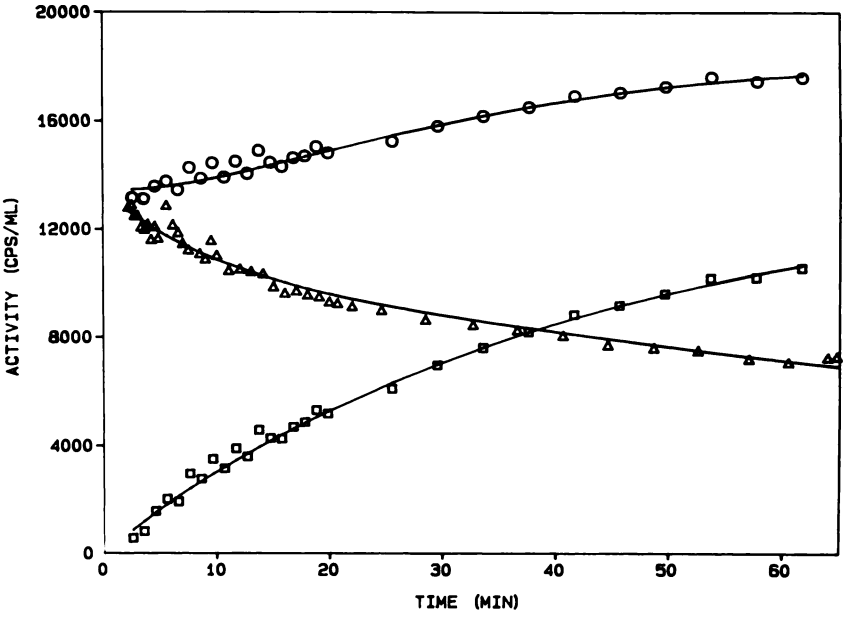

comparable to those obtained in the normal dog lung. PTCER was also determined in two patients with the adult respiratory distress syndrome (ARDS). ARDS was associated with *Pneumocystis carinii* pneumonia in one case, and tricyclic drug overdose in the other. Studies in the first patient were carried out ~10 days after initial presentation, and ~7 days after presentation in the second case. Although diffuse infiltrates were still present radiographically in both patients, and although both still required mechanical ventilation and the use of positive end-expiratory pressure, both patients had clearly improved clinically by the time of the PET study. Nevertheless, our data clearly show that PTCER remained abnormally elevated when compared with normal subjects. PTCER images from single slices from one of the patients with ARDS and from one of the normal volunteers are shown in Figure 8.

DISCUSSION

This study clearly shows the feasibility of using PET and ^{68}Ga-labeled transferrin to measure pulmonary vascular permeability (PVP) in both experimental animals and in patients with diseases known to affect PVP. We found that PTCER was approximately ten times greater in lung affected by oleic acid-induced injury than in normal areas of dog lung. Similarly, the average PTCER value in two patients with ARDS was approximately four times the average value obtained in two normal human volunteers. Our values for PTCER in normal human subjects are comparable to values previously reported by Gorin et al. (*1–2*). It is perhaps important to note that these values for the PTCER of transferrin are significantly higher than values obtained with labeled albumin, despite their similar molecular weights

FIGURE 6
Mean (±s.d.) values for regional plasma volume (Vpl), obtained in the six dogs with left lower lobe oleic acid induced injury. Note that the estimate of plasma volume does not depend on the method employed. However, Vpl did decrease significantly (* = $p < 0.05$) from the first to the second measurement, especially in injured lung.

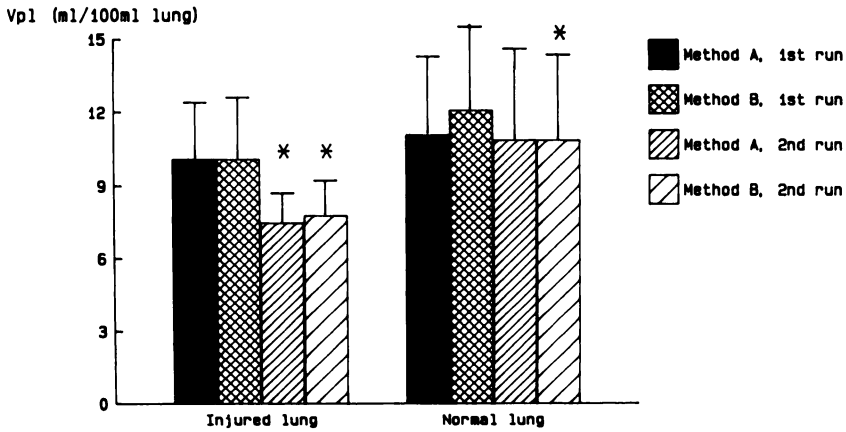

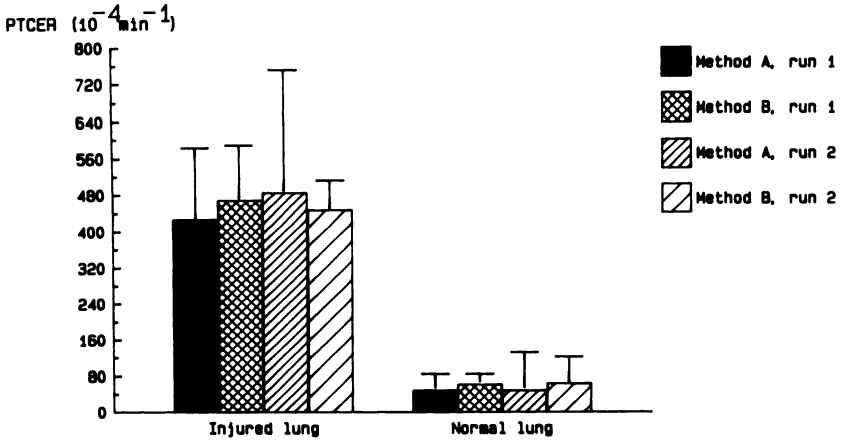

FIGURE 7
Mean (±s.d.) values for PTCER, obtained in the same dogs and lung regions represented in Figure 6. Note that the estimates of PTCER did not depend on the method employed, and did not change between the first and second measurement. Note also that values obtained in injured lung were approximately ten times those obtained in normal lung.

(*9*). Thus, our values in the ARDS patients cannot be compared directly to recently reported values obtained in other ARDS patients (*10*), using Gorin's technique with intravenously administered labeled albumin. Whether this difference in PTCER value between the two proteins is of any pathophysiologic or functional importance is not yet known. Interestingly, in our patients with ARDS, the abnormality in PVP was still evident 7–10 days after initial clinical presentation. This finding implies that the natural history of the permeability defect after lung injury is complex and may not directly predict outcome. A similar finding has been reported by others (*10,11*). Additional information of this type will obviously be of considerable interest.

Technical Considerations

The PET adaptation for measuring permeability requires several assumptions. The most important of these is that pulmonary blood volume does not change during the course of the scan. Gross changes are probably unlikely during the 1-hr scan period. In Gorin's technique, a second tracer is used to measure activity in the blood pool to avoid this particular problem. However, this approach is not possible with PET, since all positron-emitting isotopes result in annihilation photons with the same energy (511 keV). The importance of this assumption during PET studies, therefore, remains to be evaluated.

Another assumption is that the regional estimate of blood (actually plasma) volume is an appropriate index of surface area for normalizing the forward rate constant (yielding PTCER). Although the relationship of blood volume to surface area may not be linear over wide ranges of changing blood volume, still our data show that even when plasma volume decreased significantly (Fig. 6), the PTCER calculation did not change (Fig. 7). This decrease in regional plasma volume presumably represents a decrease in vascular surface area by either vasoconstriction or edematous compression of vessels during the 4-hr interval between scans.

Normalization of k_1 for differences in surface area can be accomplished with blood volume instead of plasma volume estimates. This approach has the advantage of being independent of changes in hematocrit between measurements. In this study, we chose to use plasma volume estimates since this is the approach reported by Gorin et al. and others (*1,2,22*).

To use PET to study the natural history of permeability changes during ARDS, a scheme for correct repositioning of the patients will be desirable, particularly

TABLE 1
Mean Values* for Forward (k_1) and Reverse (k_2) Transport Constants in six Dogs with Oleic Acid Induced Lung Injury to the Left Lower Lobe

Abnormal lung				Normal lung			
First measurement		Second measurement		First measurement		Second measurement	
k_1†	k_2	k_1†	k_2	k_1	k_2	k_1	k_2
0.736 ± 0.242	1.77 ± 1.17	0.581 ± 0.010	1.53 ± 0.51	0.099 ± 0.077	1.072 ± 1.900	0.118 ± 0.121	0.822 ± 1.99

* Units are 10^{-4} sec^{-1}.
† $p < 0.05$ compared with corresponding values in normal lung.
No significant difference occurred between first and second measurements.
k_1 and k_2 were estimated using Method B, as explained in the text.

TABLE 2
Values for Regional Plasma Volume (Vpl) and PTCER in Two Normal Human Volunteers and in Two Patients with ARDS

	ARDS					Normals			
	Non-dependent region		Dependent region			Non-dependent region		Dependent region	
Patient no.	Vpl*	PTCER	Vpl	PTCER	Patient no.	Vpl	PTCER	Vpl	PTCER
1	8.8	382	13.0	377	3	13.3	1	13.5	14
2	8.7	531	9.6	583	4	6.9	70	7.9	134

* Units are ml plasma/100 ml lung for Vpl and 10^{-4} min^{-1} for PTCER.

if significant inter-slice variation in PTCER values is present. This aspect of the method will require careful attention in future studies.

Comparison with Other Techniques

The advantages of measuring PVP with PET are several. First, the data can be presented in an image format. Not only is it then possible to detect regional abnormalities, but also to correlate such abnormalities with other PET-derived physiologic variables. PET can now be used to measure regional pulmonary blood flow (*12–13*), blood volume (*14*), extravascular lung water (*14–16*), density (*17–19*), ventilation (*20*), and ventilation-perfusion ratios (*21*). Some preliminary work indicates that PET may also be useful in evaluating lung metabolism. For studies of acute lung injury, a direct measure of PVP in the same region as measurements of these other variables would be an important addition.

Displaying the PET data tomographically facilitates the re-measurement of PVP over time. Without this ability, changes in PTCER measured with single probes or gamma cameras could occur because either different portions or different amounts of lung tissue were imaged. Thus, PET is ideally suited for sequential studies. PET studies of PVP should help define the natural history of permeability changes after lung injury.

PET measurements are also corrected for attenuation errors, and for artifacts due to chest wall or other soft-tissue structures (e.g., the heart). This type of correction is especially important when any type of external detection technique is used to quantitatively calculate some physiologic variable from tissue activity measurements. The quantitative accuracy of single-photon imaging techniques is always in question because such attenuation errors cannot be measured directly, which may be particularly important in the lung with its highly variable tissue density.

PET-derived estimates of PVP (the PTCER) are also normalized for regional variation in blood (plasma) volume and tissue density. Thus, ideally, the PET estimate of PTCER is independent of regional differences in surface area or varying degrees of lung inflation. This makes the PTCER measurement unique when compared with other pulmonary measurements made with PET (*14,15*).

Other techniques which have been used to evaluate PVP lack most of these advantages. Gorin's method obviously comes closest, since the PET method is a direct adaptation of his technique. However, with Gorin's method, no correction for attenuation or chest wall artifacts is made, and reproducible regional information is not easily obtained. When abnormalities of PVP are regionally inhomogeneous, the use of single probes may lead to inaccuracies, since a variable and unknown amount of abnormal and normal lung may be included under the probe.

Recently, Dauber et al. (*22*) extended Gorin's original observations by calculating PTCER with a method similar to our Method B (with albumin, not transferrin) during different types of pulmonary edema. They also calculated an "albumin leak index," in which the slope of the extravascular time-activity relationship (determined by linear regression) was divided by the intercept of the regression line with the activity axis at time zero. Using this approach (which is conceptually similar to our Method A), they found no significant difference between the two methods of evaluating vascular permeability. However, these authors as well as others (*1,2,10*) *excluded* the first 25 min of data from their analysis "to avoid any intravascular mixing artifacts." It is uncertain, however, what artifacts are actually involved. Instead, we found that the behavior of the blood curve often required a two, not a mono, exponential fit, in order to accurately describe blood-activity changes during the first portion of the data collection. This behavior apparently represents mixing of the tracer within the vascular pool and with certain rapidly exchangeable extravascular spaces (such as liver), over the first 10–20 min after isotope administration. However, as can be seen from Figures 2 and 3, if only data obtained 25 min after tracer injection is used, a serious underestimation of k_1 (and therefore, of PTCER) can certainly occur. Thus, Dauber et al. (*22*) found that PTCER differed between normal and injured lung by only three- to fourfold, whereas we found PTCER values in injured lung that were ten times control values. Therefore, we believe our analysis to be a better representation of the spectrum of permeability changes after lung injury. Our inclusion of all but the first 2 min of data after tracer injection is the most likely reason for this difference between our results and those of Dauber et al.

Sugerman and co-workers (*11*) have also used external radiation detection techniques to evaluate pulmonary vascular permeability. With their method, a gamma camera is used to measure the ratio of lung-to-heart activity over time, after injection of ^{99m}Tc-labeled albumin. Although simple to perform, the major dis-

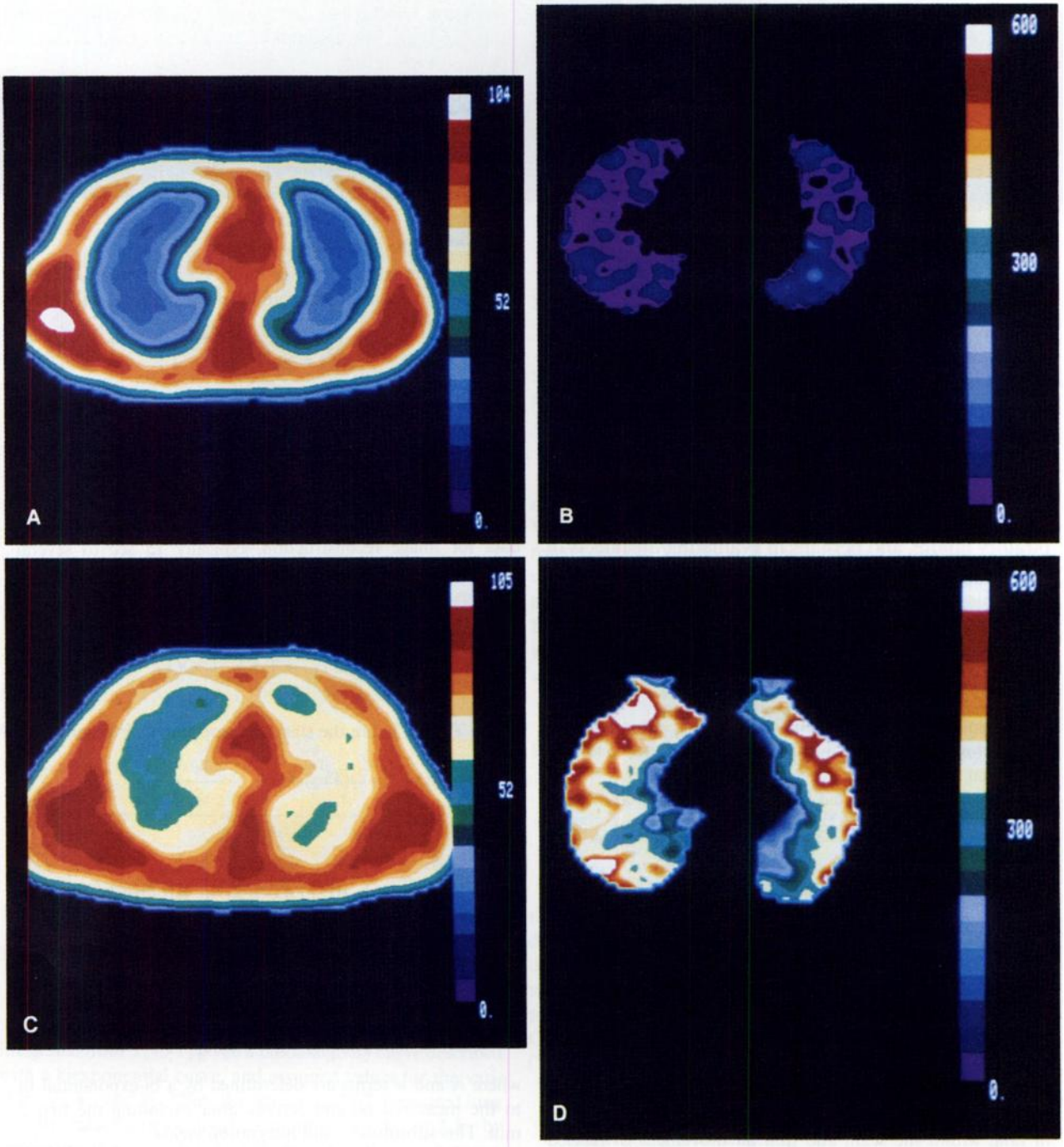

FIGURE 8
A: Single transverse tomographic slice of a transmission scan from a normal human volunteer. Color scale as in Figure 4A. Orientation of image is reversed from that shown in Figure 4A (i.e., right side of the image is left side of the subject). B: PTCER image obtained in the same slice as in A. Color scale in units of 10^{-4} min^{-1}. C: Transmission image from a patient with ARDS. Note the increase in tissue density, compared with the normal volunteer. D: PTCER image obtained in the same slice as C. Note the marked increase in PTCER compared with the normal volunteer.

advantages of this approach are the inability to display the data tomographically or to correlate it with other relevant regional physiologic measurements, such as blood flow or lung water, which can be measured by PET (*12,15*).

Finally, two other methods for evaluating PVP have been reported. In one, the permeability-surface area product for urea is calculated from indicator-dilution data obtained after a single-pass injection of several radioisotopes (*23*). Indicator dilution methods, however, are quite sensitive to regional changes in pulmonary perfusion, and produce erroneous results when regional blood flow is severely reduced. Furthermore, experimental and clinical data have both shown that

spuriously low values may be obtained when derecruitment of lung vascular surface area takes place after injury (*23,24*). Even less satisfactory is the albumin clearance technique reported by Anderson et al. (*25*), since permeability must be sufficiently abnormal that alveolar edema fluid can be obtained from the large airways. Thus, this method would not be useful except in the most florid cases of pulmonary edema.

CONCLUSIONS

We have used PET to measure the pulmonary transcapillary escape rate for ^{68}Ga-labeled transferrin in both normal and injured lung, in experimental animals and human subjects. The data obtained are reproducible and provide regional information available in an image format. Such data should be useful in distinguishing overlap syndromes involving both noncardiogenic and cardiogenic forms of pulmonary edema, in examining the natural history of permeability changes during respiratory failure, and perhaps in evaluating the effects of treatment on pulmonary vascular injury. Thus, this technique should be a valuable addition to experimental and clinical studies of acute lung injury.

ACKNOWLEDGMENTS

The authors thank John Haller and Thor Amundsen for their technical assistance, and Ms. Paige Kreienheder for her secretarial assistance.

This work was supported in part by HL 32815 and Dept. of Energy Grant DE-AC02-77EV04318.

APPENDIX

The lung tissue activity measurements obtained with PET, after in vivo labeling of transferrin with ^{68}Ga, represent activity in both vascular and extravascular compartments. The model depicted in Figure 1 can be used to interpret this data, so that forward and reverse rate constants for movement of the radiotracer between the two compartments can be calculated. With the assumptions that blood-activity measurements in peripheral blood samples will be equivalent to blood activity in lung within the scan, and that all movement of labeled protein between vascular and extravascular compartments is by passive, not active, transport, activity in the vascular compartment (Q_1) of any lung region can be described as follows:

$$Q_1(T) = B1(T) \cdot V_1, \tag{1}$$

where B1 is the measured blood activity (in counts/sec/ml blood) and V_1 is the regional blood volume in ml/100 ml lung.

On the other hand, activity in the extravascular compartment (Q_2), can be described as follows:

$$\frac{dQ_2(T)}{dt} = k_1 \cdot B1(T) - k_2 \cdot Q_2(T), \tag{2}$$

where Q_2 is the total activity, in the extravascular compartment in counts/sec/100 ml, k_1 is the forward transport rate constant in 1/sec and k_2 is the reverse transport rate constant in 1/sec. When the assumption is made that extravascular activity is zero at time zero, integration yields,

$$Q_2(T) = k_1 \cdot \int_0^T B1(t) \cdot e^{-k2 \cdot (T-t)} dt \tag{3}$$

or,

$$Q_2(T) = k_1 \cdot B1(T) * e^{-k2 \cdot T}, \tag{4}$$

where "*" is the convolution operator.

Since external detection of the labeled protein sums both vascular and extravascular compartments, Eqs. (1) and (4) are added to yield.

$$Q(T) = Q_1(T) + Q_2(T) \tag{5}$$

or

$$Q(T) = B1(T) \cdot V_1 + k_1 \cdot Bl(T) * e^{-k_2 T}, \tag{6}$$

where Q is the total tissue activity at any time. Equation (6) is analogous to that developed by Gorin et al. (*1–2*). However, a PET scan requires a finite amount of time to collect sufficient data for image reconstruction, typically 15 sec to several minutes depending on count rate. Thus, our PET adaptation requires the integration of Eq. (6).

$$PET_N(T_1 \rightarrow T_2) = \int_{T_1}^{T_2} Q(T), \tag{7}$$

where T_1 and T_2 are the start and stop times of the nth PET scan.

Substituting for Q(T) yields:

$$PET_N(T_1 \rightarrow T_2) = V_1 \cdot \int_{T_1}^{T_2} B1(T)\, dT + k_1 \int_{T_1}^{T_2} B1(T) * e^{-k_2 T}\, dt. \tag{8}$$

Since numerical integration of the plasma activity, B1(T), and the convolution term, are computationally cumbersome, B1(T) is replaced with a biexponential approximation,

$$B1(T) = A_1 \cdot e^{-\alpha_1 T} + A_2 \cdot e^{-\alpha_2 T} \tag{9}$$

where A and α terms are determined by a bi-exponential fit to the measured plasma activity after excluding the first 2 min. This substitution and integration yields

$$\begin{aligned} PET_N(T_1 \rightarrow T_2) = \Bigg[& V_1 \int_{T_1}^{T_2} A_1 \cdot e^{-\alpha_1 t}\, dt \\ & + k_1 \int_{T_1}^{T_2} \int_0^T A_1 \cdot e^{-\alpha_1 t} \cdot e^{-k_2 (T-t)}\, dt \Bigg] \\ & + \Bigg[V_1 \int_{T_1}^{T_2} A_2 \cdot e^{-\alpha_2 t}\, dt + k_1 \int_{T_1}^{T_2} \int_0^T A_2 \\ & \cdot e^{-\alpha_2 t} \cdot e^{-k_2 (T-t)}\, dt \Bigg]. \end{aligned} \tag{10}$$

and

$$PET_N(T_1 \rightarrow T_2) = \left[\frac{V_1 \cdot A_1}{\alpha_1}\right](e^{-\alpha_1 T_1} - e^{-\alpha_1 T_2}) \quad (11)$$
$$+\frac{k_1 \cdot A_1}{\alpha_1 - k_2}\left[\frac{e^{-k_2 T_1} - e^{-k_2 T_2}}{k_2} - \frac{e^{-\alpha_1 T_1} - e^{-\alpha T_2}}{\alpha_1}\right]$$
$$+\frac{V_1 \cdot A_2}{\alpha_2}(e^{\alpha_2 T_1} - e^{-\alpha_2 T_2})$$
$$+\frac{k_1 \cdot A_2}{\alpha_2 - k_2}\left[\frac{e^{-k_2 T_1} - e^{-k_2 T_2}}{k_2} - \frac{e^{-\alpha_2 T_1} - e^{-\alpha_2 T_2}}{\alpha_2}\right].$$

These equations can be simplified by the substitutions,

$$B(T_1, T_2) = A_1 \cdot \frac{(e^{-\alpha_1 T_1} - e^{-\alpha_1 T_2})}{\alpha_1} + A_2 \cdot \frac{(e^{-\alpha_2 T_1} - e^{-\alpha_2 T_2})}{\alpha_2} \quad (12)$$

and

$$C(T_1, T_2, k_2) = \frac{A_1 \cdot \left[\frac{e^{-k_2 T_1} - e^{-k_2 T_2}}{k_2} - \frac{e^{-\alpha_1 T_1} - e^{-\alpha_1 T_2}}{\alpha_1}\right]}{\alpha_1 - k_2} + \frac{A_2 \cdot \left[\frac{e^{-k_2 T_1} - e^{-k_2 T_2}}{k_2} - \frac{e^{-\alpha_2 T_1} - e^{-\alpha_2 T_2}}{\alpha_2}\right]}{\alpha_2 - k_2} \quad (13)$$

yielding the operational equation

$$PET_N(T_1 \rightarrow T_2) = V_1 \cdot B(T_1, T_2) + k_1 \cdot C(T_1, T_2, k_2). \quad (14)$$

Equation (14) calculates the expected regional lung activity, integrated from T_1 to T_2 given a blood-activity curve described with a biexponential curve, and assumed values for the variables V_1, k_1, and k_2. Thus, the sequential PET measured lung activity values can be used to estimate V_1, k_1, and k_2 by optimizing these variables to minimize the difference between the actual and expected tissue activity values. In our application, we used the Marquart parameter optimization technique (*26*) to estimate the three variables V_1, k_1, and k_2.

However, as discussed in the text (see Theory) it may be appropriate to assume k_2 is negligible. This simplifies the operational equation. Starting with Eq. (11) and assuming $k_2 = 0$,

$$PET_N(T_1 \rightarrow T_2) = \left[\frac{V_1 \cdot A_1}{\alpha_1}(e^{-\alpha_1 T_2} - e^{-\alpha_1 T_2}) + \frac{k_1 \cdot A_1}{\alpha_1}\left[(T_2 - T_1) + \frac{(e^{-\alpha_1 T_2} - e^{-\alpha_1 T_1})}{\alpha_1}\right]\right]$$
$$+\left[\frac{V_1 \cdot A_2}{\alpha_2}(e^{-\alpha_2 T_2} - e^{-\alpha_2 T_2}) + \frac{k_1 \cdot A_2}{\alpha_2}\left[(T_2 - T_1) + \frac{(e^{-\alpha_2 T_2} - e^{-\alpha_2 T_1})}{\alpha_2}\right]\right]. \quad (15)$$

Now with the one additional substitution,

$$D(T_1, T_2) = \frac{A_1}{\alpha_1}\left[T_2 - T_1 + \frac{e^{-\alpha_1 T_2} - e^{-\alpha_1 T_1}}{\alpha_1}\right] + \frac{A_2}{\alpha_2}\left[T_2 - T_1 + \frac{e^{-\alpha_2 T_2} - e^{-\alpha_2 T_1}}{\alpha_2}\right] \quad (16)$$

yields

$$PET_N(T_1 \rightarrow T_2) = V_1 \cdot B(T_1, T_2) + k_1 \cdot D(T_1, T_2), \quad (17)$$

since each nth PET scan has a unique set of nonoverlapping start and stop times, rewrite Eq. (17) to be

$$PET(N) = V_1 \cdot B(N) + k_1 \cdot D(N). \quad (18)$$

The above equation allows the calculation of the expected regional lung activity for a given PET scan when values for V_1 and k_1 are assumed. Since the equation is linear with respect to both V_1 and k_1, a linear regression analysis can be used to solve for the best V_1 and k_1 values for a given set of actual PET measured tissue activity values, represented here by $PET_m(N)$. The solution for k_1 and V_1 which minimizes the sum of the squared error in PET (expected) and PET_m (measured) is:

$$k_1 = \frac{\sum B(N) \cdot \sum(PET_m(N) \cdot D(N)) - \sum(PET_m(N) \cdot B(N))}{\sum(B(N) \cdot D(N)) \cdot \sum B(N)^2 - \sum(B(N) \cdot D(N))} \quad (19)$$

$$V_1 = \frac{\sum(PET_m(N) \cdot B(N)) - k_1 \cdot \sum(B(N) \cdot D(N))}{\sum B(N)^2}. \quad (20)$$

However, the best estimate of vascular permeability requires that the transfer rate constant, k_1, be normalized for regional differences in surface area. Since surface area per se is not directly measurable, blood volume or plasma volume is assumed to be proportional to surface area. Calculation of pulmonary transcapillary escape rate (PTCER) as defined by Gorin et al (*1–2*) requires calculation of the plasma volume, (Vpl)

$$Vpl = V_1/(1 - HCT). \quad (21)$$

Then, PTCER is calculated by

$$PTCER = k_1/Vpl. \quad (22)$$

REFERENCES

1. Gorin AB, Weidner WJ, Demling RH, et al. Noninvasive measurement of pulmonary transvascular protein flux in sheep. *J Appl Physiol* 1978; 45:225–233.
2. Gorin AB, Kohler J, DeNardo G, et al. Noninvasive measurement of pulmonary transvascular protein flux in normal man. *J Clin Invest* 1980; 66:869–877.
3. Ficke DC, Beecher DE, Hoffman GR, et al. Engineering aspects of PETT-VI. *IEEE Trans Nucl Sci* 1982; 29:474–478.
4. Yamamoto M, Ficke DC, Ter-Pogossian MM. Performance study of PETT-VI. A positron computed tomograph with 288 cesium fluoride detectors. *IEEE Trans Nucl Sci* 1982; 29:529–533.
5. Ter-Pogossian MM, Ficke DC, Yamamoto M, et al. Super-PETT-I: a positron emission tomography utilizing photon time-of-flight information. *IEEE Trans Med Imag* 1982; 1:179–187.
6. Loc'h C, Maziere M, Comar D, et al. A new generator for ionic gallium-68. *J Nucl Med* 1980; 21:171–173.
7. Hanrahan TJ, Yano Y, Welch MJ, et al. Long term study of high level Ge-68 generators. *J Label Cmpds Radiopharm* 1982; 19:1535–1536.
8. Harris WR, Pecoraro VI. Thermodynamic binding

constants for gallium transferrin. *Biochemistry* 1983; 22:292–299.
9. Gorin AB. External radio-flux detection: noninvasive measurement of protein leakage in assessing lung microvascular injury. *Ann NY Med Sci* 1982; 384:411–416.
10. Braude S, Nolop KB, Hughes JMB, et al. Comparison of lung vascular and epithelial permeability indices in the adult respiratory distress syndrome. *Am Rev Respir Dis* 1986; 133:1002–1005.
11. Sugerman HJ, Tatum JL, Burke TS, et al. Gamma scintigraphic analysis of albumin flux in patients with acute respiratory distress syndrome. *Surgery* 1984; 95:674–681.
12. Mintun MA, Ter-Pogossian MM, Green MA, et al. Quantitative measurement of regional pulmonary blood flow with positron emission tomography. *J Appl Physiol* 1986; 60:317–326.
13. Schuster DP, Marklin GF. The effect of regional lung injury or alveolar hypoxia on pulmonary blood flow and lung water measured by positron emission tomography. *Am Rev Resp Dis* 1986; 135:1037–1042.
14. Schuster DP, Mintun MA, Ter-Pogossian MM. Regional lung water and hematocrit determined by positron emission tomography. *J Appl Physiol* 1985; 59:860–868.
15. Schuster DP, Marklin GF, Mintun MA. Regional changes in extravascular lung water detected by positron emission tomography. *J Appl Physiol* 1986; 60:1170–1178.
16. Meyer GJ, Shober O, Bossaller C, et al. Quantification of regional extravascular lung water in dogs with positron emission tomography, using constant infusion of ^{15}O-labeled water. *Eur J Nucl Med* 1984; 9:220–228.
17. Schuster DP, Marklin GF, Mintun MA, et al. PET measurement of regional lung density:1. *J Comp Assist Tomogr* 1986; 10:723–729.
18. Schuster DP, Marklin GF. PET study of effect of changes in inflation and blood volume on regional lung density:2. *J Comp Assist Tomogr* 1986; 10:730–735.
19. Rhodes CG, Wollmer P, Fazio F, et al. Quantitative measurement of regional extravascular lung density using positron emission and transmission tomography. *J Comp Asst Tomogr* 1981; 5:783–791.
20. Senda M, Murata K, Itoh H, et al. Quantitative evaluation of regional pulmonary ventilation using PET and nitrogen-13 gas. *J Nucl Med* 1986; 27:268–273.
21. Valind SO, Wollmer P, Rhodes CG. Application of positron emission tomography in the lung. In: Reivich M, Alavi A, eds. Positron emission tomography. New York: Liss, 1985: 387–412.
22. Dauber IM, Pluss WT, VanGrondelle A, et al. Specificity and sensitivity of noninvasive measurement of pulmonary vascular protein leak. *J Appl Physiol* 1985; 59:564–574.
23. Brigham KL, Snell JD, Harris TR, et al. Indicator dilution lung water and vascular permeability in humans. Effects of pulmonary vascular pressure. *Circ Res* 1979; 44:523–530.
24. Rinaldo J, Borovetz HS, Mancini MC, et al. Assessment of lung injury in the adult respiratory distress syndrome using multiple indicator dilution curves. *Am Rev Respir Dis* 1986; 133:1006–1010.
25. Anderson RR, Holliday RL, Driedger AA, et al. Documentation of pulmonary capillary permeability in the adult respiratory distress syndrome accompanying human sepsis. *Am Rev Respir Dis* 1979; 119:869–877.
26. Aoki M. Introduction to optimization techniques: fundamentals and application of nonlinear programming. New York: MacMillan, 1971:99–115.